Carrier relaxation due to electron-electron interaction in coupled double quantum well structures

Marcos R. S. Tavares,[1,2] G.-Q Hai,[2] and S. Das Sarma[1]
[1]*Department of Physics, University of Maryland, College Park, Maryland 20742-4111*
[2]*Instituto de Física de São Carlos, Universidade de São Paulo, São Carlos, SP 13560-970, Brazil*
(Received 11 January 2001; published 5 July 2001)

We calculate the electron-electron interaction induced energy-dependent inelastic carrier relaxation rate in doped semiconductor coupled double quantum well nanostructures within the two-subband approximation at zero temperature. In particular, we calculate, using many-body theory, the imaginary part of the full self-energy matrix by expanding in the dynamically random-phase approximation screened Coulomb interaction, obtaining the intrasubband and intersubband electron relaxation rates in the ground and excited subbands as a function of electron energy. We separate out the single-particle and the collective excitation contributions, and comment on the effects of structural asymmetry in the quantum well on the relaxation rate. Effects of dynamical screening and Fermi statistics are automatically included in our many-body formalism rather than being incorporated in an *ad hoc* manner as one must do in the Boltzmann theory.

DOI: 10.1103/PhysRevB.64.045325 PACS number(s): 73.61.−r, 73.50.Gr, 72.10.Di

I. INTRODUCTION

Electron-electron interaction induced carrier relaxation is an important inelastic scattering process in low-dimensional semiconductor nanostructures. It is often (particularly in situations where LO phonon emission is energetically prohibited because the excited electrons do not have enough energy) the most dominant relaxation process in semiconductor quantum wells and wires, and is therefore of considerable fundamental and practical importance. Band gap engineering has led to the possibility of fabricating tunable far infrared quantum well cascade lasers (QCL's) and efficient quantum well infrared photodetectors (QWIP's), where inelastic carrier relaxation via electron-electron interaction is a crucial (perhaps even decisive) process in determining device operation and feasibility.[1] For QCL and QWIP operations it is the intersubband inelastic relaxation that turns out to be the primary rate-limiting scattering process. For other proposed devices, such as the planar hot electron transistors or related two-dimensional (2D) high-speed devices, intrasubband relaxation is the important process. A thorough quantitative understanding of intra- and intersubband relaxation due to electron-electron interaction is therefore important for the successful realization of these devices. In addition to this practical technological motivation arising from QCL, QWIP, and other proposed band-gap-engineered quantum well devices, there is also an obvious fundamental reason for studying inelastic Coulomb scattering in 2D quantum well systems. Inelastic electron-electron scattering determines the 2D quasiparticle spectral width, as determined, for example, in tunneling measurements, through the imaginary part of the electron self-energy function.[2]

In this article we use a many-body approach in calculating the inelastic relaxation rate of 2D electrons confined in GaAs-$Al_xGa_{1-x}As$ semiconductor quantum well structures. Our work is a multisubband generalization of the earlier work[3] by Jalabert and Das Sarma, who considered only intrasubband relaxation within a single subband model. We consider both intra- and intersubband relaxation in the two lowest subbands, and consider both single-well and coupled double-well structures. An additional important issue addressed in our work is the effect of structural asymmetry in the quantum well on the relaxation rate. This is in fact a potentially significant factor in the fabrication of QCL and QWIP structures since asymmetry could lead to the opening of new electron-electron interaction channels in the inelastic intersubband relaxation as we discuss below in this article.

The central quantity we calculate in this work, within the leading-order dynamically screened Coulomb interaction expansion (the so-called GW approximation in the multisubband situation), is the imaginary part of electronic on-shell self-energy matrix, M, in the quantum well subband index $(i,j,$ etc.). The subband self-energy in the multisubband situation is, in general, off-diagonal, reflecting the breaking of the translational invariance along the growth (z) direction (we take the x-y plane to be the 2D plane with all wave vectors in this paper being 2D wave vectors in the x-y plane). The off-diagonal self-energy, $\mathrm{Im}(M_{ij})$, incorporates in an intrinsic many-body manner the possibility of electron-electron-interaction-induced intersubband scattering (both virtual and real) of carriers. We believe that in the doped situation of our interest, where the quantum well subbands are occupied by many electrons, the many-body self-energy approach is also a reasonable technique in calculating the inelastic carrier relaxation rate in spite of the Boltzman equation approach, where the scattering rates are usually calculated using Fermi's golden rule. The dynamical screening inherent in the many-electron system, which affects the calculated inelastic scattering rates in profound and highly nontrivial way, is automatically incorporated in our many-body GW expansion, whereas inclusion of dynamical screening in Fermi's golden rule type formula is done by replacing the bare interaction by a screened interaction in an *ad hoc* manner.

Our theory, as mentioned above, is based on the so-called GW self-energy approximation[3,4] where the electron self-energy M is obtained in a leading order expansion of the dynamically screened Coulomb interaction $W \equiv V^s$, where the superscript s denotes dynamical screening of the bare electron-electron interaction matrix V in the multisubband

situation. We use the RPA to obtain the dynamical screened interaction V^s, i.e., $V^s \equiv \varepsilon^{-1} V$, with $\varepsilon \equiv 1 - V\Pi$, where Π is the leading-order (i.e., noninteracting) electron polarizability matrix. We also approximate the electron Green's function G by the noninteracting Green's function G^0, making our formal expression for the self-energy matrix to be

$$M \sim \int G^0 V^s, \tag{1}$$

where the integral involves integrating over all internal momentum and energy variables as well as summing over all internal subband indices (and spin). Putting the subband (matrix) indices explicitly in Eq. (1), we get

$$\text{Im } M_{ij} = \text{Im} \sum_{lm} \int G^0_{lm} V^s_{ilmj}. \tag{2}$$

We note, however, that G^0, being the noninteracting Green's function, is necessarily diagonal in subband indices (i.e., an electron cannot undergo intersubband scattering in the absence of interaction):

$$G^0_{lm} \sim G^0_{ll} \delta_{lm}. \tag{3}$$

Then, Eq. (2) becomes

$$\text{Im } M_{ij} = \sum_l \int \text{Im}\,[G^0_{ll} V^s_{illj}], \tag{4}$$

with

$$V^s_{illj} = (\varepsilon^{-1} V)_{illj}. \tag{5}$$

Equations (4) and (5) are the central formal equations we use in our theory to obtain the inelastic relaxation time τ, remembering that the scattering rate Γ and the relaxation time τ are connected by

$$\tau = \frac{\hbar}{2\Gamma}, \tag{6}$$

where

$$\Gamma = |\text{Im } M|. \tag{7}$$

We emphasize that the inelastic relaxation time τ defined by Eq. (6) and calculated in this paper is an energy relaxation time (and not a momentum relaxation time, as, for example, will enter the calculation of the mobility of the system). The inelastic relaxation time calculated in this paper defines the lifetime of a single-particle energy eigenstate in the system. Due to Coulomb scattering among the electrons the single-particle stationary states are well-defined only over a limited time scale and our calculated τ is a measure of this lifetime arising from electron-electron interaction.

In Eqs. (6) and (7), $\Gamma = |\text{Im } M|$ is calculated on-shell, i.e., the quasiparticle self-energy defines Γ. To demonstrate how Eq. (4) may, in principle, differ from the Fermi golden rule approach we consider the specific two-subband model of interest to us in this paper. Then $i,j,l = 1,2$ with only subband 1, the ground subband, and the subband 2, the first excited subband being considered in the theory assuming all other subbands to be substantially higher in energy, making negligible contributions to the self-energies of the lowest two subbands. We also assume the square well structure to be symmetric, so that parity is a good quantum number in the problem which makes all ''off-diagonal'' interaction matrix elements vanish[5] by virtue of parity conservation with the only nonzero elements of V^s being $V^s_{1111}, V^s_{2222}, V^s_{1212}$, and V^s_{1122} (note that $V^s_{1221} = V^s_{2112}$ and $V^s_{1122} = V^s_{2211}$ by symmetry). In this situation Eq. (4) implies that

$$\text{Im } M_{12} = \text{Im } M_{21} = 0 \tag{8}$$

and

$$\text{Im } M_{22} \sim \int \text{Im}\,[G^0_{11} V^s_{2112} + G^0_{22} V^s_{2222}]. \tag{9}$$

We note that the dynamically screened interaction matrix element V^s_{1122} is not explicitly present in Eq. (9). On the other hand, a Fermi golden rule approach[6] will explicitly include such a V^s_{1122} term, because it seems to arise from the direct Coulomb interaction V_{1122} between an electron in subband 1 and an electron in subband 2 without any intersubband scattering. We mention, however, that dynamical screening of V_{2222} produces an effective V_{2211} term in our theory since dynamical screening proceeds through virtual creation of electron-hole pairs.

We have calculated the energy-dependent inelastic relaxation rate at $T = 0$ for a two-subband (1 and 2) GaAs-$Al_xGa_{1-x}As$ quantum well system with a total electron density $N_e = 2 \times 10^{11}$ cm^{-2} for the following five distinct situations. (i) Two coupled symmetric quantum wells of width 150 Å each with interwell tunneling induced by a tunneling barrier of height 228 meV and width 30 Å. Here the lowest two subbands are the so-called symmetric (bonding) and antisymmetric (antibonding) levels with energies $E_1 = 15.35$ meV and $E_2 = 17.03$ meV, respectively. The third level $E_3 = 60.53$ meV is sufficiently high to be ignored ($E_{F1} = E_F - E_1 = 4.28$ meV; $E_{F2} = E_F - E_2 = 2.61$ meV), with both subbands 1 and 2 occupied by carriers. These results are presented in Sec. III A below. (ii) Two coupled asymmetric quantum wells with interwell tunneling [the same as in (i) above], with one well of width 150 Å and the other of width 140 Å, leading to $E_1 = 15.93$ meV and $E_2 = 18.55$ meV ($E_{F1} = E_F - E_1 = 4.75$ meV; $E_{F2} = E_F - E_2 = 2.13$ meV). Again, the next excited subband $E_3 = 62.86$ meV is high enough to be ignored. These results are presented in Sec. III A below. (iii) Two coupled identical symmetric quantum wells of width 150 Å each with no interwell tunneling (i.e., the interwell barrier is taken to be infinity) and with a barrier width of 30 Å . Here, $E_1 = E_2 = 23.87$ meV (this degeneracy arises because the two wells are identical and there is no tunneling), $E_{F1} = E_{F2} = E_F - E_1 = E_F - E_2 = 3.44$ meV, and the next subband $E_3 = 96$ meV is sufficiently high in energy to be neglected. These results are presented in Sec. III B below. (iv) The same as in the last case with no interwell tunneling but an asymmetric situation with the two wells being different. One has a width of 150 Å and the other a width of 142.4 Å so that the subband Fermi

energies $E_{F1}=E_F-E_1=4.75$ meV and $E_{F2}=E_F-E_2=2.13$ meV, which are the same as in (ii) above. In this situation $E_1=23.87$ meV, $E_2=26.49$ meV (again E_3 can be neglected). Furthermore, to keep the average distance between the two electron layers the same as in (ii), we choose a barrier of width 28.8 Å. These results are presented in Sec. III B below in comparison with those in (ii). (v) A single symmetric quantum well of width 300 Å and a barrier height 228 meV, which leads to the lowest two subbands at $E_1=4.88$ meV, $E_2=19.51$ meV, and the Fermi energy $E_{F1}=E_F-E_1=6.88$ meV (with $E_F<E_2$, so that the second subband is empty). In this situation, the next excited subband, $E_3=43.74$ meV, is high enough in energy to be neglected. These results are present in Sec. III C below. Our reason for studying the five different classes of systems described above is that we are interested in understanding the effects of interwell tunneling and structural asymmetry on the electron relaxation rate. In particular, asymmetry breaks parity conservation, making the off-diagonal matrix elements of Coulomb interaction (e.g., $V_{1112}, V_{1121}, V_{1211}, V_{2111}, V_{2221}, V_{2212}, V_{2122}, V_{1222}$ all of which are zero in the symmetric situation) nonzero, leading to new inelastic relaxation channels not present in symmetric structures. For the sake of brevity we present results for a single representative carrier density and well parameters in each of the five cases. Our theory could be easily generalized to obtain finite temperature relaxation rates. Note that our goal here is to provide a qualitative understanding of how various physical parameters affect Coulomb scattering rates in 2D quantum wells.

The plan of this article is the following. In Sec. II we present a brief theory with working formulas; in Sec. III we provide our numerical results and discussions; we conclude in Sec. IV with a summary.

II. THEORY

Our basic theory is outlined in the Introduction, where the formal expression for the self-energies to be calculated were given. Our central GW random-phase approximation (RPA) expression[7] for the self-energy can be explicitly written out by using the noninteracting subband Green's function

$$G^0_{ij}(\omega,k)=\delta_{ij}[\omega-E_i(k)+E_F]^{-1}, \tag{10}$$

where ω is a complex frequency ($\hbar=1$), and $E_i(k)=E_i+k^2/2m^*$ is the noninteracting subband one-electron energy dispersion. Using Eq. (10) in Eqs. (4) and (5), and carrying out the internal frequency integration, and taking the imaginary part after the on-shell analytic continuation, we get

$$\begin{aligned}\mathrm{Im}\,M_{ij}(k)=&\frac{1}{(2\pi)^2}\sum_l\int d^2\mathbf{q}\\ &\times\mathrm{Im}[V^s_{illj}|(\mathbf{q},\xi_l(\mathbf{k}+\mathbf{q}))-\xi_i(\mathbf{k})]\\ &\times\{\theta(\xi_i(\mathbf{k})-\xi_l(\mathbf{k}+\mathbf{q}))\\ &-\theta(-\xi_l(\mathbf{k}+\mathbf{q}))\},\end{aligned} \tag{11}$$

where the on-shell subband energy $\xi_i(\mathbf{k})$ is given by

$$\xi_i(\mathbf{k})=E_i(\mathbf{k})-E_F, \tag{12}$$

and $\theta(x)=0(1)$, for $x<0(>0)$, is the Heaviside step function. The dynamically screened Coulomb interaction is given by [see Eq. (5)]

$$V^s_{ijlm}=(\varepsilon^{-1}V)_{ijlm}, \tag{13}$$

with the multisubband RPA approximation[7] defined by the dielectric matrix

$$\varepsilon_{ijlm}=(1-V_{ijlm}\Pi^0_{lm}), \tag{14}$$

where V_{ijlm} is the bare Coulomb interaction matrix element in the subband representation, and Π^0_{ij}, the noninteracting polarizability, is given by

$$\Pi^0_{ij}(\mathbf{k},\omega)=-2\int\frac{d^2\mathbf{q}}{(2\pi)^2}\frac{f_i(\mathbf{k}+\mathbf{q})-f_i(\mathbf{k})}{\omega-E_i(\mathbf{k}+\mathbf{q})+E_j(\mathbf{k})}, \tag{15}$$

where $f_i(\mathbf{k})$ is the Fermi distribution function in the ith subband. In this paper, we take the impurity-scattering-induced background broadening γ as being a small phenomenological damping parameter which equivalent to be working in the clean limit. We are therefore restricting ourselves to high mobility quantum wells with small impurity-scattering-induced level broadening.

Using Eqs. (11)–(15) it is straightforward to calculate the imaginary part of the on-shell self-energy. For the sake of completeness, we show below the detailed expressions for $\mathrm{Im}\,M_{ij}$ in the GW approximation for the two-subband model:

$$\mathrm{Im}\,M_{11}(k)=\sigma_{1111}(k)+\sigma_{1221}(k), \tag{16}$$

$$\mathrm{Im}\,M_{12}(k)=\sigma_{1112}(k)+\sigma_{1222}(k), \tag{17}$$

$$\mathrm{Im}\,M_{21}(k)=\sigma_{2111}(k)+\sigma_{2221}(k) \tag{18}$$

and

$$\mathrm{Im}\,M_{22}(k)=\sigma_{2112}(k)+\sigma_{2222}(k). \tag{19}$$

Here,

$$\begin{aligned}\sigma_{1111}(k)=&\frac{1}{(2\pi)^2}\int d^2\mathbf{q}\{\mathrm{Im}[V^s_{1111}(\mathbf{q},A)]\\ &\times[\theta(-A)-\theta(-\xi_1(\mathbf{k}+\mathbf{q}))]\},\end{aligned} \tag{20}$$

$$\begin{aligned}\sigma_{1221}(k)=&\frac{1}{(2\pi)^2}\int d^2\mathbf{q}\{\mathrm{Im}[V^s_{1221}(\mathbf{q},A+\omega_0)]\\ &\times[\theta(-A-\omega_0)-\theta(-\xi_2(\mathbf{k}+\mathbf{q}))]\},\end{aligned} \tag{21}$$

$$\begin{aligned}\sigma_{1112}(k)=&\frac{1}{(2\pi)^2}\int d^2\mathbf{q}\{\mathrm{Im}[V^s_{1112}(\mathbf{q},A)]\\ &\times[\theta(-A)-\theta(-\xi_1(\mathbf{k}+\mathbf{q}))]\},\end{aligned} \tag{22}$$

$$\sigma_{1222}(k)=\frac{1}{(2\pi)^2}\int d^2\mathbf{q}\{\mathrm{Im}\,[V^s_{1222}(\mathbf{q},A+\omega_0)]\times[\theta(-A-\omega_0)-\theta(-\xi_2(\mathbf{k}+\mathbf{q}))]\},\quad(23)$$

$$\sigma_{2111}(k)=\frac{1}{(2\pi)^2}\int d^2\mathbf{q}\{\mathrm{Im}\,[V^s_{2111}(\mathbf{q},A-\omega_0)]\times[\theta(-A+\omega_0)-\theta(-\xi_1(\mathbf{k}+\mathbf{q}))]\},\quad(24)$$

$$\sigma_{2221}(k)=\frac{1}{(2\pi)^2}\int d^2\mathbf{q}\{\mathrm{Im}\,[V^s_{2221}(\mathbf{q},A)]\times[\theta(-A)-\theta(-\xi_2(\mathbf{k}+\mathbf{q}))]\},\quad(25)$$

$$\sigma_{2112}(k)=\frac{1}{(2\pi)^2}\int d^2\mathbf{q}\{\mathrm{Im}\,[V^s_{2112}(\mathbf{q},A-\omega_0)]\times[\theta(-A+\omega_0)-\theta(-\xi_1(\mathbf{k}+\mathbf{q}))]\},\quad(26)$$

and

$$\sigma_{2222}(k)=\frac{1}{(2\pi)^2}\int d^2\mathbf{q}\{\mathrm{Im}\,[V^s_{2222}(\mathbf{q},A)]\times[\theta(-A)-\theta(-\xi_2(\mathbf{k}+\mathbf{q}))]\},\quad(27)$$

where $\omega_0=E_2-E_1$ is the subband energy difference, $A\equiv A(\mathbf{q},\mathbf{k})=(2kq\,\cos\eta+q^2)/2m^*$ with η being the angle between $\mathbf{k}$ and $\mathbf{q}$; and $m^*=0.07m_e$ being the GaAs conduction band electron effective mass. Now, we define the *total* inelastic Coulomb scattering rate for an electron with wave vector k (i.e., an energy of $k^2/2m^*$ with respect to the subband bottom) in the subband 1 and 2 as

$$\sigma_1(k)=\mathrm{Im}\,M_{11}(k)+\mathrm{Im}\,M_{12}(k)\quad(28)$$

and

$$\sigma_2(k)=\mathrm{Im}\,M_{21}(k)+\mathrm{Im}\,M_{22}(k).\quad(29)$$

It is important to realize that the screened potentials V^s_{ijlm} for $j\neq l$ do not appear in Eqs. (20)–(27) and, consequently, do not explicitly contribute to scattering rate. They are implicitly induced in the theory through dynamical screening[8] as discussed before. Furthermore, all screened interactions V^s_{ijlm} involved in Eqs. (20)–(27) are obtained from the relation between the bare electron-electron potential[7]

$$V_{ijlm}(q)=\frac{2\pi e^2}{q\varepsilon_0}\int dz\int dz'\,\phi_i(z)\phi_j(z)\times e^{-q|z-z'|}\phi_l(z')\phi_m(z')$$

and the inverse matrix of the dynamical dielectric function $\varepsilon_{ijlm}(q,\omega)$ [see Eqs. (13) and (14), where the indices $i,j,l,m=1,2$]. These bare Coulomb potentials $V_{ijlm}(q)$ are calculated here by using both the one-electron wave function $\phi_i(z)$ and the subband energy E_i obtained through the numerical solution of the Schrödinger equation in the z direction for the specific quantum well confinement potential. Furthermore, the potential $V_{ijlm}(q)$ can be separated into intra- and intersubband terms, and understood as follows: (i) intralayer (intrasubband) interactions $V_{1111}(q)=V_A$, $V_{2222}(q)=V_B$, and $V_{1122}(q)=V_{2211}(q)=V_C$ represent those scattering events which the electrons remain in their original well (subband); (ii) interlayer (intersubband) interactions $V_{1212}(q)=V_{2121}(q)=V_{1221}(q)=V_{2112}(q)=V_D$ represent scattering in which both electrons change their well (subband) indices; and (iii) intrawell-interwell (subband) interactions $V_{1112}(q)=V_{1121}(q)=V_{1211}(q)=V_{2111}(q)=V_J$ and $V_{2212}(q)=V_{2221}(q)=V_{1222}(q)=V_{2122}(q)=V_H$ indicate the scattering in which only one of the electrons suffers the interwell (intersubband) transition.

For each wave vector k, the two-dimensional $\mathbf{q}$ integrals in Eqs. (20)–(27) are performed within the planes determined through the variables $\mathbf{q}$ and A in the screened interactions V^s_{ijlm}. The integration domains of q and η (in A) variables are restricted by the two θ functions appearing in the integrals in Eqs. (20)–(27). The integrals involving V^s_{1111} and V^s_{1112} are performed within the planes formed by those regions in the q space where

$$\theta(-A)-\theta(-\xi_1(\mathbf{k}+\mathbf{q}))\neq 0,\quad(30)$$

while the integrals involving V^s_{1221} and V^s_{1222} are calculated within the planes defined by

$$\theta(-A-\omega_0)-\theta(-\xi_2(\mathbf{k}+\mathbf{q}))\neq 0.\quad(31)$$

In the same way, the integrals involving V^s_{2222} and V^s_{2221} are performed within the planes defined by

$$\theta(-A)-\theta(-\xi_2(\mathbf{k}+\mathbf{q}))\neq 0,\quad(32)$$

and, finally, for V^s_{2112} and V^s_{2111} the integrating plane is defined by

$$\theta(-A+\omega_0)-\theta(-\xi_1(\mathbf{k}+\mathbf{q}))\neq 0.\quad(33)$$

The inelastic scattering rates in Eqs. (20)–(27) vanish outside each corresponding integrating plane, which means that the momentum and energy conservation cannot be simultaneously obeyed for such values of $(\mathbf{k},\mathbf{k}+\mathbf{q})$, and therefore no Coulomb scattering is allowed there. It is easy to see that these integrals are nonvanishing only if the corresponding integrating plane contains either some part of the single-particle excitation continuum or some branch representing the collective excitations (plasmons) in the 2D q plane. This is of course expected since a finite scattering rate must involve real excitations, which in this case are single-particle and collective plasmon excitations.

III. NUMERICAL RESULTS AND DISCUSSIONS

A. Coulomb coupled bilayers with interwell tunneling

We consider first two coupled symmetric identical quantum wells of same width $W_1=W_2=150$ Å with an interwell tunneling induced by a barrier of height 228 meV and width 30 Å. The total electron density $N_e=n_1+n_2=2\times10^{11}$ cm^{-2} in all structures studied in this paper, with

n_1 and n_2 being the density in the subband 1 and 2, respectively. For these sample parameters, the Fermi wave vectors in the first and second subband are $k_{F1}^{sy} \simeq 0.88 \times 10^6$ cm^{-1} and $k_{F2}^{sy} \simeq 0.69 \times 10^6$ cm^{-1}, respectively (the superscript sy stands for symmetric). Here, both subbands 1 and 2 (symmetric and antisymmetric, respectively) are occupied by carriers with $n_1 \simeq 1.23 \times 10^{11}$ cm^{-2} and $n_2 \simeq 0.77 \times 10^{11}$ cm^{-2}.

The plasmon dispersion relation is determined by the roots of the determinantal equation $\det|\varepsilon_{ijlm}(q,\omega)| = 0$, which, after some algebra, can be rewritten as

$$\varepsilon_{\text{intra}}\varepsilon_{\text{inter}} - [(1 - V_A\Pi_{11}^0)V_H^2\Pi_{22}^0 + (1 - V_B\Pi_{22}^0)V_J^2\Pi_{11}^0 - 2V_CV_JV_H\Pi_{11}^0\Pi_{22}^0(\Pi_{12}^0 + \Pi_{21}^0)] = 0, \quad (34)$$

where

$$\varepsilon_{\text{intra}} = (1 - V_A\Pi_{11}^0)(1 - V_B\Pi_{22}^0) - V_C^2\Pi_{11}^0\Pi_{22}^0 \quad (35)$$

and

$$\varepsilon_{\text{inter}} = 1 - V_D(\Pi_{12}^0 + \Pi_{21}^0). \quad (36)$$

For notational simplicity, we do not explicitly write the energy and wave vector dependence in Eqs. (34)–(36). For the present symmetric situation, the unscreened Coulomb potential $V_J = V_H = 0$ by virtue of parity symmetry, because the wave functions $\phi_1(z)$ and $\phi_2(z)$ are symmetric and antisymmetric functions of z, respectively. According to Eq. (34), therefore, the plasmons dispersion relation in our symmetric bilayer structure is determined by the roots of the equation $\varepsilon_{\text{intra}}\varepsilon_{\text{inter}} = 0$, i.e., either $\varepsilon_{\text{intra}} = 0$ corresponding to the 2D intrasubband plasmons, or $\varepsilon_{\text{inter}} = 0$ corresponding to the intersubband plasmons.

There are four roots of $\varepsilon_{\text{intra}} = 0$. Two of them are shown in Fig. 1(a) by the solid lines indicating the intrasubband plasmon modes (1,1) and (2,2). Notice that, for each solid line, there is a corresponding dashed line that is also the root of the same equation always lying in the corresponding single-particle excitation continuum. It is well known that the plasmon modes indicated by the dashed lines inside the single-particle continua are strongly Landau damped by single-particle excitations and will be ignored in the following discussion. Furthermore, the intersubband plasmon mode (1,2) comes from the roots of $\varepsilon_{inter} = 0$. The wave functions $\phi_1(z)$ and $\phi_2(z)$ are schematically shown in the inset by the solid and dot lines, respectively. Notice that, one is always able to separate the intra and inter-subband plasmon modes in structures that are invariant under space inversion. In addition, the intrasubband plasmons are not Landau damped by intersubband single-particle excitations (SPE's) and vice versa in symmetric bilayer systems. The single-particle continua SPE_{11} (intrasubband SPE) and SPE_{12} (intersubband SPE) in Fig. 1(a) are those regions where $\text{Im}\{\Pi_{11}^0(q,\omega)\} \neq 0$ and $\text{Im}\{\Pi_{12}^0(q,\omega)\} \neq 0$, respectively. For the sake of simplicity, we will not indicate the continuum SPE_{22} in this paper because it lies totally inside the continuum SPE_{11}. Moreover, we claim that the plasmon mode (2,2) should be strongly damped by single-particle excitations in the SPE_{11} continuum and will also be ignored in the following qualitative scattering rate discussion. Our numerical results of course include all contributions as obtained by evaluating the 2D integrals in Eqs. (20)–(27).

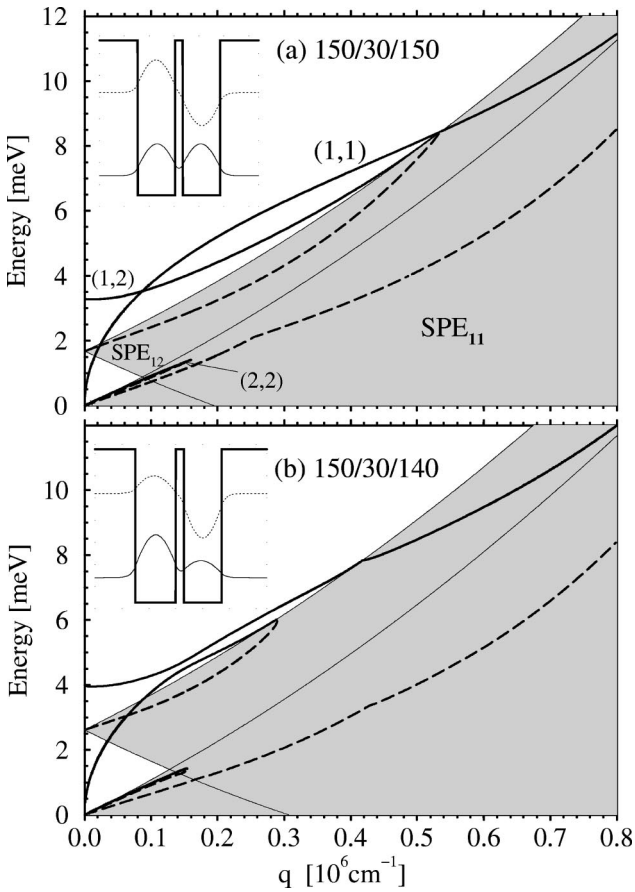

FIG. 1. Plasmon dispersions in two coupled GaAs/$Al_{0.3}Ga_{0.7}As$ quantum wells of widths (a) $W_1 = W_2 = 150$ Å (symmetric) and (b) $W_1 = 150$ Å and $W_2 = 140$ Å (asymmetric); and separated by a barrier of width 30 Å . For the symmetric (asymmetric) situation the energy separation between the two subbands is $\omega_0 = 1.68$ meV ($\omega_0 = 2.62$ meV). The shadow areas present the single-particle excitation regions $SPE_{nn'}$ where $\text{Im}\{\Pi_{nn'}^0(q,\omega)\} \neq 0$. Each structure is shown in the inset where $\phi_1(z)$ and $\phi_2(z)$ are schematically shown by the solid and dot lines, respectively.

Figure 1(b) shows the same plasmon dispersion relation as in Fig. 1(a) but now in two coupled *asymmetric* quantum wells with interwell tunneling. Here, one well is of width 150 Å and the other is of width 140 Å. For these parameters, the Fermi wave vector in the subband 1 and 2 are $k_{F1}^a \simeq 0.93 \times 10^6$ cm^{-1} and $k_{F2}^a \simeq 0.62 \times 10^6$ cm^{-1}, respectively (the superscript a stands for asymmetric). Both subbands are occupied with $n_1 \simeq 1.37 \times 10^{11}$ cm^{-2} and $n_2 \simeq 0.63 \times 10^{11}$ cm^{-2}. In this asymmetric situation, the plasmon modes are obtained directly from the roots of Eq. (34). We show in Fig. 1(b) all these roots. We mention that it does not make sense naming the solid lines as pure intra- or intersubband plasmon modes because the structural asymmetry leads to a strong coupling (or mixing) between them, and this intrasubband-intersubband mode coupling eliminates the simplicity of Fig. 1(a). The solid line that is of finite frequency as $q \to 0$ in Fig. 1(b) is the intersubbandlike plasmon

mode (1,2). This mode enters the continuum SPE_{12} at $q \simeq 0.42\times10^6$ cm^{-1} and should be, in principle, Landau damped. For small values of q, we find the same number of roots as in the symmetric situation. The interactions V_J and V_H are finite in the asymmetric case and are responsible for the strong mixing between the intrasubbandlike plasmon mode (1,1) and the intersubbandlike mode (1,2) around $q \cong 0.18\times10^6$ cm^{-1}. Moreover, when the asymmetry is introduced, the depolarization shift (i.e., the shift of the intersubband plasmon from the subband energy separation E_{21}) in the intersubbandlike plasmon (1,2) at $q=0$ decreases. We point out that these roots of Eq. (34) do not provide a complete description of the plasmon modes in asymmetric bilayer structures. A detailed theoretical calculation of the dynamical structure factor giving the plasmon spectral weight provides a complete picture of the collective mode spectra and can be obtained using our multisubband theory.

Having studied the plasmon dispersion relations we now investigate in Fig. 2(a) the corresponding total inelastic Coulomb scattering rate $\sigma_1(k)$ (thick solid line) and $\sigma_2(k)$ (thick dashed line) of fast electrons in the subband 1 and 2, respectively, as a function of wave vector k in our symmetric bilayer structure. The symbols on the thin lines identify the contributions to $\sigma_1(k)$ and $\sigma_2(k)$ coming from the emission of single-particle and collective excitations individually. The dynamically screened Coulomb interaction components entering in Eqs. (20)–(27) can be calculated from Eqs. (13) and (14). After some algebra, we get

$$V^s_{1111}=\frac{V_A(1-V_B\Pi^0_{22})+V_C^2\Pi^0_{22}}{\varepsilon_{\rm intra}}, \tag{37}$$

$$V^s_{2222}=\frac{V_B(1-V_A\Pi^0_{11})+V_C^2\Pi^0_{11}}{\varepsilon_{\rm intra}}, \tag{38}$$

and

$$V^s_{1221}=V^s_{2112}=\frac{V_D}{\varepsilon_{\rm inter}}. \tag{39}$$

For the symmetric well case the off-diagonal components of the Coulomb potential all vanish by parity: $V^s_{1112}=V^s_{1121}=V^s_{1211}=V^s_{2111}=V^s_{2221}=V^s_{2212}=V^s_{2122}=V^s_{1222}=0$ because $V_J=V_H=0$ for symmetric systems. Therefore, according to Eqs.(20)–(29), the total inelastic scattering rates in the subband 1 and 2 are

$$\sigma_1(k)=\sigma_{1111}+\sigma_{1221} \tag{40}$$

and

$$\sigma_2(k)=\sigma_{2222}+\sigma_{2112}, \tag{41}$$

respectively. The terms σ_{1111}, σ_{1221}, σ_{2222}, and σ_{2112} involve integrations of the interactions V^s_{1111}, V^s_{1221}, V^s_{2222} and V^s_{2112}, respectively, in Eqs. (20), (21), (27), and (26). The self-energy components in Eqs. (22)–(25) are zero in the symmetric case. *Intrasubband* contributions to the scattering rates arise from the terms σ_{1111} and σ_{2222}, while *intersubband* contributions are due to the terms σ_{1221} and σ_{2112}. The

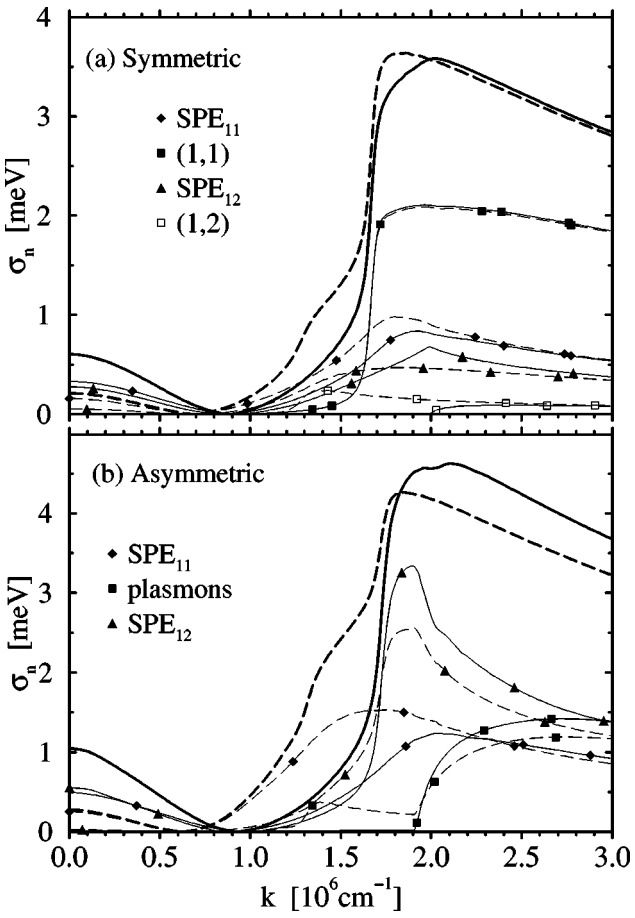

FIG. 2. Total inelastic Coulomb scattering rate of electrons in our coupled bilayer (a) symmetric and (b) asymmetric structures. The thick solid and thick dashed lines denote the total scattering rate $\sigma_n(k)$ for $n=1$ and 2, respectively. The symbols on the thin lines represent each contribution to the total calculated scattering: diamonds standing for the SPE_{11} contribution, the filled squares stand for the intrasubband (1,1) plasmon contribution, triangles stand for the SPE_{12} contribution, and opaque squares stand for the intersubband (1,2) plasmon contribution.

contributions coming from the plasmon modes (filled-square lines) are obtained separately by excluding the continua SPE_{11} and SPE_{12} from the numerical integrations, whereas contributions coming only from the single-particle continua are obtained by numerically evaluating Eqs. (21) and (26) only for the region representing each continuum. Single-particle excitations contribute for all values of wave vectors k. However, neither intra- nor intersubband plasmon mode contributes to the scattering rates close to $k^{\rm sy}_{F1}$ or $k^{\rm sy}_{F2}$. These collective modes provide excitation channels for inelastic relaxation only above some threshold wave vectors. The intrasubband plasmon mode (1,1) begins to contribute to either $\sigma_1(k)$ or $\sigma_2(k)$ when the wave vector is larger than the same threshold $k^{\rm sy}_{11}\simeq 1.65\times10^6$ cm^{-1}. On the other hand, the contribution coming from the plasmon mode (1,2) has a different threshold for each scattering rate. This mode begins contributing to $\sigma_1(k)$ and $\sigma_2(k)$ when the wave vector is larger than the thresholds $k^{\rm sy}_{12}\simeq 1.25\times10^6$ cm^{-1} and $k^{\rm sy}_{12'}\simeq 2.0\times10^6$ cm^{-1}, respectively (notice that $k^{\rm sy}_{F2}<k^{\rm sy}_{F1}<k^{\rm sy}_{12}$

$<k_{11}^{sy}<k_{12'}^{sy}$). Obviously, these thresholds depend on the particular choice of sample parameters. In the present paper, they are smooth (instead of being a very sharp threshold) because we are considering the impurity-induced constant $\gamma=0.2$ meV in our numerical evaluation. These thresholds become much sharper for smaller values of γ without any other substantive changes in our numerical results.

Figure 2(b) shows the same results as in Fig. 2(a) but for the asymmetric bilayer system of Fig. 1(b). In contrast to the symmetric case, where we were able to separately obtain the inter- and intrasubband plasmon modes through the roots of $\varepsilon_{\text{inter}}=0$ and $\varepsilon_{\text{intra}}=0$, respectively; the coupled plasmon dispersion in the asymmetric system is obtained directly from the numerical roots of Eq. (34) in which the bare off-diagonal Coulomb interactions V_J and V_H are now nonvanishing. The terms in Eq. (34) involving V_J and V_H are responsible for the mixing between the inter- and intrasubband plasmon modes and for not allowing the contributions coming from the intra- and intersubbandlike plasmon modes (1,1) and (1,2) to be picked up completely separated from each other in the scattering rate. Notice that the dynamically screened Coulomb potential V_{ijlm}^{s} is a full 16×16 matrix (for the two-subband model—in general, it is an $n^4\times n^4$ matrix for an n-subband problem) in the present situation and is obtained from Eq. (13), which involves the dielectric matrix $\varepsilon_{ijlm}(q,\omega)$ and the bare Coulomb interactions V_A, V_B, V_C, V_D, V_J, and V_H (all of which are finite in this strongly coupled asymmetric bilayer structure).[9] Therefore, both inelastic scattering rates $\sigma_1(k)$ and $\sigma_2(k)$ in the asymmetric case contain all terms shown in Eqs. (20)–(27), which are finite in this situation. For the sake of clarity and to understand Fig. 2(b) in the same way as done for Fig. 2(a), we choose to show three contributions to the inelastic scattering rates $\sigma_1(k)$ and $\sigma_2(k)$ in Fig. 2(b) separately: the single-particle excitations in the continua (i) SPE_{12} (up triangles) and (ii) SPE_{11} (diamonds); and (iii) the plasmon mode segment outside these continua (filled squares). The filled squares in Fig. 2(b) represent contributions coming from those segments of the plasmon modes that lie outside any single-particle excitation continua [see Fig. 1(b)]. Contributions coming from the plasmon segments lying inside each continuum have been kept in our numerical work along with the single-particle excitation contributions because it is essentially numerically impossible to separate the two in this regime. We should mention that, due to the fact that one is not able to eliminate the contributions coming from the overdamped plasmon modes lying inside the Landau continua, the thin lines in Fig. 2(b) only serve as a qualitative illustration.[10]

B. Coulomb coupled bilayers with no interwell tunneling

Now we investigate the two Coulomb coupled identical symmetric quantum wells of width $W_1=W_2=150$ Å each with *no* interwell tunneling (i.e., the interwell barrier is taken to be infinity) and with a barrier width of 30 Å. Here, the Fermi wave vectors in the two wells are of the same value, i.e., $k_{F0}=k_{F1}=k_{F2}\simeq0.79\times10^6$ cm^{-1} (or, equivalently, $n_1=n_2=10^{11}$ cm^{-2}). Notice that the indices 1 and 2 should now be treated as well indices since there is no tunneling-induced bonding-antibonding states. As we mentioned in the Introduction, an energy degeneracy arises in this case, i.e., $E_1=E_2$ because the two wells are identical with no interwell tunneling. If there is no tunneling, the bare Coulomb potential components $V_J=V_H=V_D=0$ and the polarizability $\Pi_{12}^0=\Pi_{21}^0=0$ independent of whether the bilayer structure is symmetric or not. Besides, for this symmetric no-tunneling bilayer structure, the bare Coulomb potential $V_A=V_B$ by symmetry and the polarizability $\Pi_{11}^0=\Pi_{22}^0=\Pi_0$ due to the fact that the densities in each well are identical.

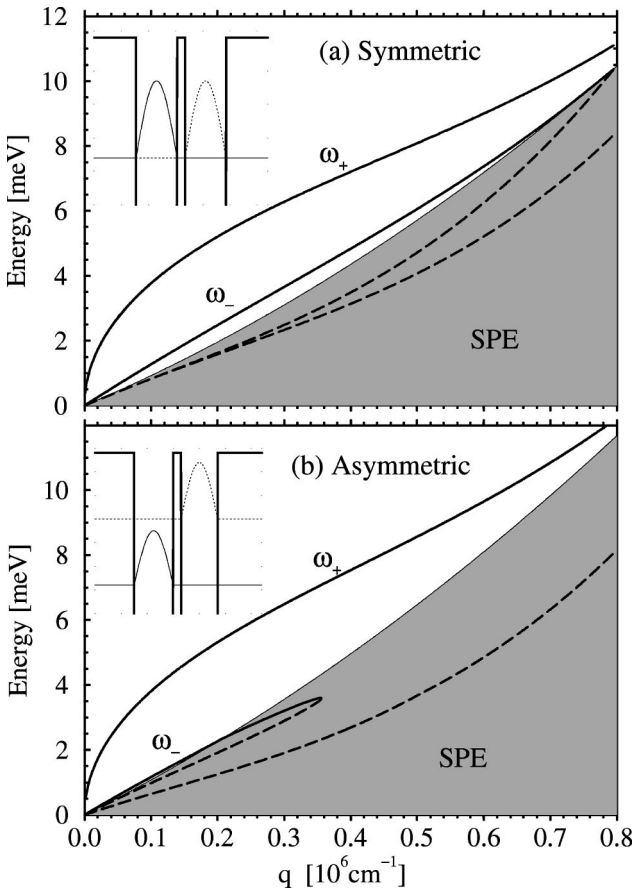

FIG. 3. Plasmon dispersions in two coupled with no interwell tunneling GaAs/$Al_{0.3}Ga_{0.7}$As quantum wells of widths (a) $W_1=W_2=150$ Å and (b) $W_1=150$ Å (symmetric) and $W_2=142.4$ (asymmetric) Å, and separated by an infinity barrier of width 28.87 Å. The shadow areas present the single-particle excitation regions $\text{SPE}_{11'}$ where $\text{Im}\{\Pi_{11'}^0(q,\omega)\}\neq0$. Each structure is shown in the inset where $\phi_1(z)$ and $\phi_2(z)$ are schematically shown by the solid and dotted lines, respectively.

According to Eqs. (34)–(36), therefore, the plasmon dispersion relation should be obtained only from the roots of

$$\varepsilon_{\text{nt}}^{\text{sy}}=(1-V_A\Pi_0)^2-V_C^2\Pi_0^2=0. \tag{42}$$

Here, the subscript (superscript) nt (sy) stands for no tunneling (symmetric). As shown in Fig. 3(a), we find four roots of Eq. (42). The solid curves correspond to the in-phase optical, $\omega_+(q)$, and the out-of-phase acoustic, $\omega_-(q)$, plasmon

modes in the bilayer structure.[11] These $\omega_{\pm}(q)$ modes have been observed[12] in multilayer semiconductor systems via inelastic light scattering spectroscopic experiments. They represent in-phase and out-of-phase interlayer density fluctuation modes: the out-of-phase acoustic mode, $\omega_{-}(q\rightarrow 0) \sim O(q)$ represents densities in the two layers fluctuating out of phase with a linear wave vector dispersion and the in-phase optical mode, $\omega_{+}(q\rightarrow 0)\sim \sqrt{N_e q}$, represents densities in the two layers fluctuating in phase with the usual 2D plasma dispersion. The dashed lines represent the collective modes that should be strongly Landau damped by the single-particle excitation continuum SPE, i.e., the region where $\mathrm{Im}\{\Pi_0(q,\omega)\}\neq 0$.

Figure 3(b) shows the same quantities as in Fig. 3(a) but for an asymmetric no-tunneling situation with the two wells being different, one with a width of $W_1=150$ Å and the other a width of $W_2=142.4$ Å. In this case, our no-tunneling bilayer structure is no longer invariant under space inversion and, consequently, the energy level degeneracy is broken, leading to the energy $E_1<E_2$. Besides, the bare Coulomb potential V_A is now different from V_B. As we discussed before, the two wells now have different charge densities but we consider the whole system still being in equilibrium. Furthermore, the Fermi wave vector in the first and second subbands is the same as indicated before, i.e., k_{F1}^a and k_{F2}^a, respectively. Because of the densities in the two wells being different from each other, the polarizability $\Pi_{22}^0\neq\Pi_{11}^0$. The shadow area in Fig. 3(b) is the single-particle excitation continuum in the wider quantum well, i.e., the region where $\mathrm{Im}\{\Pi_{11}^0(q,\omega)\}\neq 0$. The plasma dispersion relation is now given by the roots of the Eq. (35). Note that all plasma modes in the zero tunneling system are by definition intrasubband plasmons in our model where higher subbands are neglected.

As shown in Fig. 3(b), we again find four roots of such an equation and consider that the dashed lines should be strongly Landau damped modes since they are inside the single-particle continua. Furthermore, it does not make sense, in principle, to define the solid lines in Fig. 3(b) as pure acoustic or optical plasmon modes because the asymmetry leads to a difference between the electron densities in each layer. Now, the wider well has 30% more electrons than the narrower one, and, consequently, the densities in the two layers are not fluctuating exactly either in phase or out of phase. The solid lines in Fig. 3(b) are the approximate acoustic- and optical-like plasmon modes with the strict distinction meaningful only in the long-wavelength limit. Due to the structural asymmetry the acousticlike plasmon mode enters the SPE continuum at a smaller wave vector, leading to significant Landau damping of the acoustic plasmon mode by single-particle excitations in the asymmetric bilayer system. In the single-particle continuum of the layer 2 (the narrower well) the acousticlike plasmon mode is completely suppressed and we find no acousticlike mode in the $\mathrm{Im}\{\Pi_{22}^0(q,\omega)\}\neq 0$ regime. In general the acousticlike plasmon mode is found to be much more sensitive to small asymmetry effects than the optical-like plasmon mode.[13] This is physically reasonable and should be experimentally tested via inelastic light scattering experiments.

Now we concentrate on the investigation of the scattering rates $\sigma_1(k)$ and $\sigma_2(k)$ in the symmetric bilayer structure with no tunneling. As the bare Coulomb potential $V_J=V_H=V_D=0$, it is straightforward to see that only V_{1111}^s and V_{2222}^s are finite in the screened Coulomb interaction matrix V^s for a bilayer structure without any tunneling. Therefore the scattering rates in Eqs. (21)–(26) all vanish by symmetry in this case. The only nonvanishing terms to be calculated are σ_{1111} and σ_{2222} in Eqs. (20) and (27), respectively. Furthermore, as we discussed before, we have the polarizability $\Pi_{11}^0=\Pi_{22}^0=\Pi_0$ and the bare potential $V_A=V_B$ for identical (i.e., symmetric case) quantum wells. According to Eqs. (37) and (38), therefore, the screened Coulomb potential is given by

$$V_{1111}^s=V_{2222}^s=\frac{V_A(1-V_A\Pi^0)+V_C^2\Pi^0}{\varepsilon_{nt}^{sy}} \tag{43}$$

in the present situation of a symmetric bilayer system with no interwell tunneling. In fact, the total inelastic Coulomb scattering $\sigma_1(k)$ and $\sigma_2(k)$ are identical because the two wells are identical with the same density. The thick line shown in Fig. 4(a) represents the total inelastic scattering rate, which is equal $[\sigma_1(k)=\sigma_{1111}=\sigma_2(k)=\sigma_{2222}]$ in both subbands, as a function of the wave vector k. To show separately the contributions coming from the emission of plasmons (squares) and single-particle excitations (diamonds), we again exclude the region where $\mathrm{Im}[\Pi_0(q,\omega)]\neq 0$ from the numerical calculations to obtain the plasmon contribution. Single-particle excitations again contribute at all values of the wave vector, whereas the plasmons begin contributing to the scattering rate for wave vectors k larger than the Fermi wave vector k_{F0}. There are clearly two thresholds wave vectors in the plasmon contribution (squares), one at $k=k_{\mathrm{ac}}^{\mathrm{sy}}\simeq 1.25\times 10^6\ \mathrm{cm}^{-1}$ and other at $k=k_{\mathrm{op}}^{\mathrm{sy}}\simeq 1.65\times 10^6\ \mathrm{cm}^{-1}$. These are the thresholds for the emission of the acoustic and the optical plasmon, respectively. The substantial difference between Figs. 4(a) and 2(a) demonstrates the strong effect of tunneling on the inelastic scattering rates in bilayer structures. This is one of the important qualitative results in our paper.

Figure 4(b) shows the same results as in Fig. 4(a) but for the asymmetric bilayer structure without tunneling. As we discussed before, the asymmetry leads to $\Pi_{22}^0\neq\Pi_{11}^0$. Furthermore, the bare Coulomb potential $V_A\neq V_B$ and, therefore according to Eqs. (37) and (38), the screened Coulomb potential $V_{1111}^s\neq V_{2222}^s$ in the asymmetric case. In this situation, $\sigma_1(k)=\sigma_{1111}$ (thick solid line) and $\sigma_2(k)=\sigma_{2222}$ (thick dashed line) represent the total inelastic Coulomb scattering rates in the wider and narrower layer, respectively. They are different from each other because the two wells have different widths and densities in the asymmetric situation. Again, we separate the different contributions (by plasmons and by SPE) by excluding the single-particle excitation continuum SPE from the numerical calculations to obtain the plasmon contribution. It is important to point out again that the

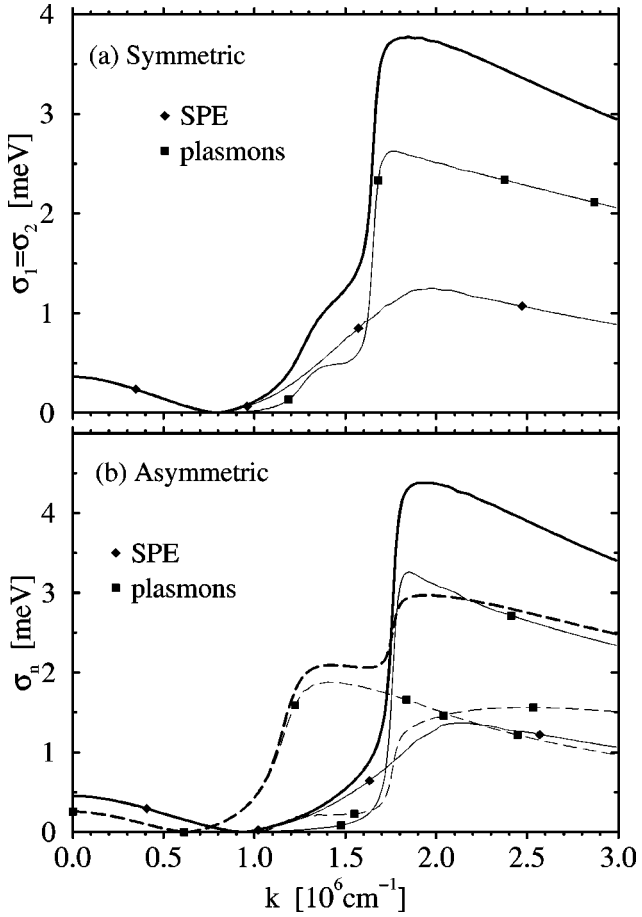

FIG. 4. Total inelastic Coulomb scattering rate of electrons in our coupled bilayer (a) symmetric and (b) asymmetric structures with no tunneling. In (b), the thick solid and thick dashed lines denote the total scattering rate $\sigma_n(k)$ for $n=1$ and 2, respectively. The symbols on the thin lines represent each contribution to the total scattering: diamonds stand for the SPE contributions, and the filled squares stand for the plasmon contributions.

squares in Fig. 4(b) represent contributions coming from the emission of undamped plasmon modes whose frequency $\omega(q)$ lies outside the continuum SPE [see Fig. 3(b)]. There is only one threshold wave vector $k\simeq 1.71\times 10^6$ cm^{-1} in the thin solid line (squares) corresponding the plasmon contribution to $\sigma_1(k)$. This threshold is due to the emission of the optical-like plasmon mode shown in Fig. 3(b). We also find that the thin solid line (diamonds) corresponding to the SPE contribution to $\sigma_1(k)$ does not contain any contribution coming from the acousticlike plasmon mode. As a matter of fact, there is no contribution to $\sigma_1(k)$ in Fig. 4(b) coming from the emission of the acousticlike plasmon mode at all because the integral in $\sigma_1(k)$ does not contain any segment representing the acousticlike plasmon mode which is heavily Landau damped in the asymmetric situation under consideration. On the other hand, the thin dashed line (squares), corresponding to the plasmon contribution to $\sigma_2(k)$, clearly has two threshold wave vectors $k\simeq 1.15\times 10^6$ cm^{-1} and $k\simeq 1.76\times 10^6$ cm^{-1}, which characterizes the emission of the acoustic- and optical-like plasmon mode, respectively. Thus, in the asymmetric case, the acoustic-like plasmon modes contribute to carrier scattering $\sigma_2(k)$ in the narrower well but not to $\sigma_1(k)$ in the wider well by virtue of strong Landau damping. The difference between Figs. 2(b) and 4(b) represents the strong effect of tunneling on the second component of the inelastic scattering rates $\sigma_2(k)$ in bilayer asymmetric structures.

C. Single symmetric quantum well

We now consider (for the sake of comparison) a single symmetric GaAs-Al$_x$Ga$_{1-x}$As quantum well of width 300 Å, barrier height 228 meV, and with the same total electron density $N_e=2\times 10^{11}$ cm^{-2} as used before. These sample parameters lead to the Fermi wave vector in the first subband $k_{F1}^{\rm single}\simeq 1.13\times 10^6$ cm^{-1} with only one subband occupancy. Here, the second subband is empty, which leads to $\Pi_{22}^0=0$. As we discussed before, only the bare Coulomb potential V_A, V_B, V_C, and V_D are finite because $V_J=V_H=0$ in symmetric structure. According to Eqs. (35) and (36), therefore, the intra- and intersubband plasmon modes are obtained from the roots of the equations

$$\varepsilon_{\rm intra}^{\rm single}=(1-V_A\Pi_{11}^0)=0$$

and

$$\varepsilon_{\rm inter}^{\rm single}=1-V_D(\Pi_{12}^0+\Pi_{21}^0)=0.$$

Taking $\Pi_{22}^0=0$ (unoccupied excited subband) in Eqs. (37), (38), and (39) we get

$$V_{1111}^s=\frac{V_A}{\varepsilon_{\rm intra}^{\rm single}}, \tag{44}$$

$$V_{2222}^s=\frac{V_B(1-V_A\Pi_{11}^0)+V_C^2\Pi_{11}^0}{\varepsilon_{\rm intra}^{\rm single}}, \tag{45}$$

and

$$V_{1221}^s=V_{2112}^s=\frac{V_D}{\varepsilon_{\rm inter}^{\rm single}}. \tag{46}$$

Again in this case, the screened Coulomb potential $V_{1112}^s=V_{1121}^s=V_{1211}^s=V_{2111}^s=V_{2221}^s=V_{2212}^s=V_{2122}^s=V_{1222}^s=0$ by symmetry because $V_J=V_H=0$. Therefore, as we discussed in the Sec. III A, the total inelastic scattering rates in the first and the second subband are given by Eqs. (40) and (41), respectively. In the same way as done for the bilayer structures, we present the scattering rates $\sigma_1(k)$ and $\sigma_2(k)$ in Fig. 5 in the thick solid and thick-dashed lines, respectively. The symmetric nature of the single-well system enables us to separate out the different contributions to the scattering rates as discussed before. We find that contributions to $\sigma_1(k)$ come mainly from the emission of both the intrasubband plasmons (1,1) and the intrasubband single-particle excitations SPE$_{11}$. The emission of intersubband excitations turn out to make negligible contributions to the scattering because of the sufficiently large energy gap between the two subbands ($\omega_0=E_{21}=14.63$ meV). For this particular choice of

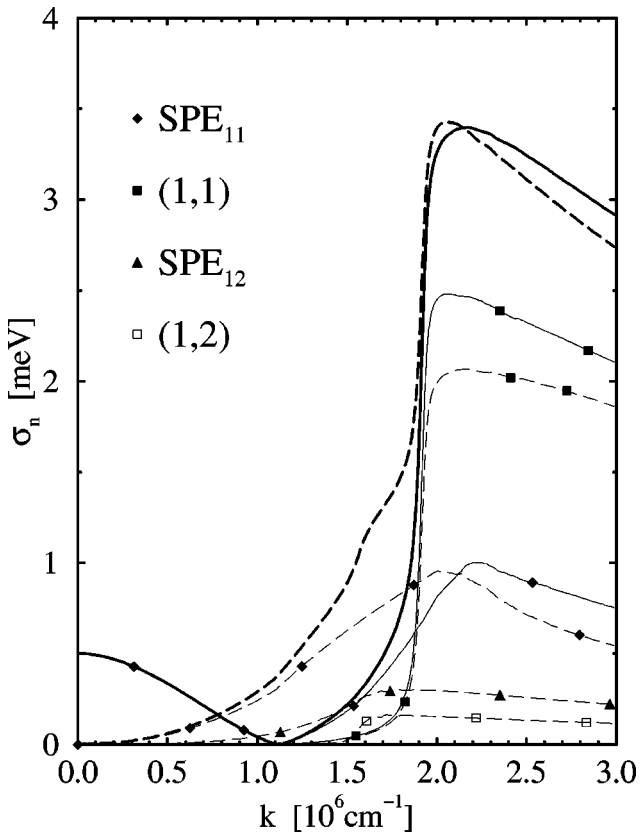

FIG. 5. Total inelastic Coulomb scattering rate of electrons in a single quantum well. The thick solid and thick dashed lines denote the total scattering rate $\sigma_n(k)$ for $n=1$ and 2, respectively. The symbols on the thin lines stand for the same as indicated in Fig. 2(a).

the sample parameters, σ_{1111} turns out to be much larger than σ_{1221}, implying that the carrier relaxation process in the ground subband is almost entirely via intrasubband scattering. Another important point in Fig. 5 is that inter- and intrasubband plasmon modes as well as intra- and intersubband single-particle excitations contribute to the total inelastic scattering rate $\sigma_2(k)$ in the second subband. Notice that, in contrast to the behavior of $\sigma_1(k)$, the total inelastic scattering rate in the second subband $\sigma_2(k)$ does not vanish for any wave vectors k. This is due the fact that there is no Fermi surface in the second subband. This should lead to qualitatively different effects in the measured carrier injected in the second subband compared with that in the ground subband.[14] This lifetime, which is inversely proportional to the total inelastic scattering rate $\sigma_2(k)$, should be finite for all finite wave vectors in the excited empty subband.

IV. CONCLUSIONS

We have developed a theory for calculating the inelastic relaxation rate for Coulomb scattering in coupled bilayer structures in semiconductor double quantum well systems. We use a many-body theory based on a multisubband generalized GW approximation with the inelastic scattering rate defined by the magnitude of the imaginary part of the on-shell electron self-energy. Effects of dynamical screening, mode coupling, and Fermi statistics are naturally included in our many-body theory. We demonstrate the usefulness of our theory by obtaining results for general representative two-subband model systems: Coulomb coupled bilayer GaAs-Al_xGa_{1-x}As double quantum well structures both with and without interwell tunneling and also with and without interwell asymmetry in the system. Our theory naturally allows for distinguishing various physical mechanisms contributing to the inelastic scattering rate: intra- and intersubband contributions. We provide a critical qualitative discussion of these various contributions to scattering and comment on the effect of interwell tunneling and structural asymmetry in bilayer quantum wells.

ACKNOWLEDGMENTS

M.R.S.T. is supported by FAPESP, Brazil. The work at the University of Maryland is supported by the ONR, U.S. G.Q.H. acknowledges CNPq from Brazil for partial support.

[1] See, for example, the Proceedings of the 5th International Conference on Intersubband Transition in Quantum Wells (ITQW) [Physica E **7** (1/2) (2000)] for the latest status of the field.

[2] L. Zheng and S. Das Sarma, Phys. Rev. B **54**, 2751 (1996); P. Sotirelis, Paul von Allmen, and Karl Hess, *ibid.* **47**, 12 744 (1993).

[3] R. Jalabert and S. Das Sarma, Phys. Rev. B **40**, 9723 (1989).

[4] L. Hedin, Phys. Rev. **139**, A796 (1965); see also G. D. Mahan, *Many-Particle Physics* 2nd ed. (Plenum, New York, 1981).

[5] J. K. Jain and S. Das Sarma, Phys. Rev. B **36**, 5949 (1987); S. Das Sarma, *ibid.* **29**, 2324 (1984).

[6] S.-C. Lee and I. Galbraith, Phys. Rev. B **59**, 15 796 (1999).

[7] S. Das Sarma *et al.*, Phys. Rev. B **19**, 6397 (1979); B. Y. K. Hu and S. Das Sarma, *ibid.* **48**, 5469 (1993); M. R. S. Tavares, S. Das Sarma, and G. Q. Hai, *ibid.* **63**, 045324 (2001).

[8] G. Q. Hai, N. Studart, F. M. Peeters, P. M. Koenraad, and J. H. Wolter, J. Appl. Phys. **80**, 5809 (1996).

[9] We do not present here the full $16\times16V^s_{ijlm}$ or ε_{ijlm} matrix in the asymmetric situation because it is not particularly illuminating. In fact, it is much more convenient to evaluate everything numerically using the matrix inversion shown in Eqs. (13) and (14).

[10] Notice that, it is extremely difficult, by numerical means, to exclude contributions from those segments of the damped plasmon modes lying inside each single-particle continua when we are calculating the single-particle excitation contributions to the scattering rate.

[11] S. Das Sarma and A. Madhukar, Phys. Rev. B **23**, 805 (1981); D. Olego, A. Pinczuk, A. C. Gossard, and W. Wiegmann, *ibid.* **25**, 7867 (1982); D. S. Kainth, D. Richards, H. P. Hughes, M. Y.

Simmons, and D. A. Ritchie, *ibid.* **57**, R2065 (1998).

[12] A. Pinczuk, M. G. Lamont, and A. C. Gossard, Phys. Rev. Lett. **56**, 2092 (1986); G. Fasol, N. Mestres, H. P. Hughes, A. Fischer, and K. Ploog, *ibid.* **56**, 2517 (1986); S. Das Sarma and E. H. Hwang, *ibid.* **81**, 4216 (1998).

[13] G. Q. Hai and Marcos R. S. Tavares, Phys. Rev. B **61**, 1704 (2000); Marcos R. S. Tavares and G. Q. Hai, *ibid.* **61**, 7564 (2000).

[14] S. Q. Murphy, J. P. Eisenstein, L. N. Pfeiffer, and K. W. West, Phys. Rev. B **52**, 14 825 (1995).